Computers & Geosciences 37 (2011) 1391–1399

Contents lists available at ScienceDirect

Computers & Geosciences

journal homepage: www.elsevier.com/locate/cageo

Numerical assessment of boulder transport by the 2004 Indian ocean tsunami in Lhok Nga, West Banda Aceh (Sumatra, Indonesia)

N.A.K. Nandasena [a], Raphaël Paris [b,c], Norio Tanaka [a,d,*]

[a] Graduate School of Science and Engineering, Saitama University, 255 Shimo-okubo, Sakura-ku, Saitama 338-8570, Japan
[b] Clermont Université, 63000 Clermont-Ferrand, France
[c] CNRS, GEOLAB, 63057 Clermont-Ferrand, France
[d] Institute for Environmental Science and Technology, Saitama University, 255 Shimo-okubo, Sakura-ku, Saitama 338-8570, Japan

ARTICLE INFO

Article history:
Received 9 June 2010
Received in revised form
31 January 2011
Accepted 3 February 2011
Available online 8 March 2011

Keywords:
Calcareous boulders
Current velocity
Numerical simulation
Finite difference method
Field observation

ABSTRACT

Few studies have been conducted on modeling boulder transport by tsunamis despite considerable research on the analysis of boulder deposits. A detailed description of the derivation of governing equations for boulder transport in submerged, partially submerged, and subaerial (not in contact with fluid) is presented, and then a numerical model is proposed to solve the governing equations in one dimension. Subsequently, the model is used to analyze the transport of calcareous boulders detached from a seawall in Lhok Nga (northwestern Sumatra, Indonesia) by the 2004 Indian Ocean tsunami. A few simulated transport distances match field observations, but the others are higher than the field measurements. Clast-to-clast interactions at the inception of transport would have a major impact on changes in transport distance, dissipating the energy in impulses as destruction of the seawall releases different sizes of boulders with different velocities. Moreover, surface microtopographical effects could completely stop the transport prematurely. The difference between the simulated results and the field observations is partly attributed to limitations of the numerical model. No landward fining was observed in the field measurements, but numerically predicted results showed a reasonable trend of landward fining.

1. Introduction

An accurate method to estimate the magnitude (or "size") of past tsunamis from their deposits, including boulders, is a major issue to be developed in studies on tsunami hazard assessment. The pretransport environment, transport mode, transport distance, properties of the boulder, hydraulic force associated with tsunamis, and topography are essential elements in the analysis. However, the accuracy of the final outcome could depend on good field observations, identification of sources, and recognition of complex transport behavior of boulders in the turbulent fluid flow. Lorang (2000) proposed equations to predict the threshold entrainment mass for a boulder beach during storms. Hansom et al. (2008) modeled the process of cliff-top erosion and deposition under extreme storm waves by experimental and numerical studies. Goff et al. (2010) showed by numerical assessments that the tsunami flow depths required for deposition of the New South Wales boulders from suspension are most probably physically unrealistic. Kogure and Matsukura (2010) developed models for wave-induced stress due to wave force on a cliff to determine the critical height of a tsunami wave to collapse the cliff. Nott (1997) developed hydrodynamic equations to assess the pretransport environment of a coastal boulder transported by tsunamis or storm surges, and further specified different conditions for a boulder based on its position on the ground, including submerged, subaerial, and joint bounded (Nott, 2003). These equations, which included the effects of drag, lift, inertia, gravity, and buoyant forces on the boulder, were derived mainly by applying the moment of the aforesaid hydrodynamic forces to the boulder to predict whether the boulder would be overturned or not by the fluid impact, and they have been used widely in subsequent studies (e.g., Mastronuzzi and Sanso, 2004; Nott, 2004; Williams and Hall, 2004; Kennedy et al., 2007; Lange et al., 2006; Scicchitano et al., 2007; Mhammdi and Medina, 2008; Spiske et al., 2008; Scheffers et al., 2008; Maouche et al., 2009; Pignatelli et al., 2009; Barbano et al., 2010; Etienne and Paris, 2010; Paris et al., 2010; Switzer and Burston, 2010; Lorang, in press). Noormets et al. (2004) developed equations focusing on dislodgment, emplacement, and transport of boulders. Pignatelli et al. (2009) developed a simple relationship to find the transport distance of a boulder based on Nott's equations. If one uses Nott's equations to determine the

* Corresponding author at: Saitama University, Graduate School of Science and Engineering, 255 Shimo-okubo, Sakura-ku, Saitama 338-8570, Japan.
Tel./fax: +81 48 858 3564.
E-mail address: tanaka01@mail.saitama-u.ac.jp (N. Tanaka).

0098-3004/$ - see front matter © 2011 Elsevier Ltd. All rights reserved.
doi:10.1016/j.cageo.2011.02.001

magnitude of tsunamis or storm surges, the possibility of underestimating is high because the equations consider only the initial transport due to rolling/overturning, but theoretically the initial transport mode can also be sliding or saltation depending on the magnitude (current velocity) of the tsunami (Nandasena et al., in press). Thus, the results of Nott's equations should be applied with caution (Morton et al., 2006; Goto et al., 2009a; Switzer and Burston, 2010; Hall et al., 2010; Bourgeois and Mac Innes, 2010; Benner et al., 2010), especially for hazard assessment and interpretation of coastal boulder accumulations (Paris et al., 2010). Moreover, Nott's equations do not take the actual transport of the boulder into account. Therefore, to analyze the temporal variations of boulder velocity and flow field to which a boulder is subjected when it is transported, an advanced numerical approach is needed. A numerical model for the transport of a boulder developed by Noji et al. (1993) was extended to two dimensions by Imamura et al. (2001), and Goto et al. (2009b, 2010) employed the model to simulate the boulder transport by the 2004 Indian Ocean tsunami at Pakarang Cape, Thailand. The model consists of depth-integrated continuity and momentum equations to simulate the tsunami-induced flow and a momentum equation to analyze boulder transport under submerged conditions. According to Imamura et al. (2008) the model has some limitations and needs further improvements. When a boulder is entrained by tsunami-induced currents, the submerged, partially submerged, and subaerial (not in contact with fluid) conditions would be three consecutive stages experienced by the boulder. The boulder could be transported in the partially submerged condition depending on the size and density of the boulder.

Therefore, in this study, governing equations for boulder transport in submerged, partially submerged, and subaerial conditions are derived, and then a new numerical scheme to solve the governing equations is proposed. Subsequently, the model is used to analyze the transport of calcareous boulders detached from a seawall by the 2004 Indian Ocean tsunami in Lhok Nga (northwestern Sumatra, Indonesia).

2. Theory of boulder transport (one dimension)

2.1. Components of force on a boulder

Boulder transport due to fluid impact is complex, but the complexity is simplified with assumptions as follows. A boulder is regarded as a rectangular prism, and its motion is restricted to sliding and saltation on a bed. The bed is impermeable and not eroding. Forces acting on the boulder are limited to drag, lift, inertia, friction, and reduced gravity force (vector summation of self-weight and buoyancy). The tsunami force is perpendicular to the boulder face derived from the long and short axes (a and h_b; Fig. 1) where F_d is the drag force, F_m the inertia force, F_f the friction force, F_l the lift force, u the current velocity (flow velocity) near the boulder, U the boulder velocity, h the water depth near the boulder, F_g the reduced gravity force, a, b, and h_b the dimensions of boulder ($a > b > h_b$), α the slope of bed, ς the water surface elevation measured from a datum, and z the bed elevation measured from the datum.

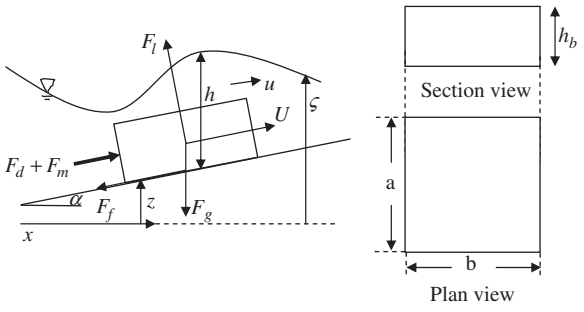

Fig. 1. Detailed sketch of a boulder transported on a slope by a tsunami and its associated forces.

The forces acting can be written using the concept of relative velocity as follows.

Drag force,

$$F_d = (1/2)\rho C_d A_d |u-U|(u-U), \tag{1}$$

where C_d is the coefficient of drag, A_d the drag area (ah_b), and ρ the density of water.

Inertia force,

$$F_m = \rho vol_b(Du/Dt) + \rho C_a vol_b(Du/Dt - dU/dt), \tag{2}$$

where C_a is the coefficient of added mass or virtual mass, vol_b the volume of boulder (abh_b), and Du/Dt the total horizontal acceleration of water near the boulder, which can be expanded as follows in one dimension.

$$Du/Dt = \partial u/\partial t + u\partial u/\partial x. \tag{3}$$

Lift force,

$$F_l = (1/2)\rho C_l A_l (u-U)^2, \tag{4}$$

where C_l is the coefficient of lift and A_l the lift area(ab).

It is assumed that the lift force exists when the water pressure drops at the top of the boulder (Luccio et al., 1998). Thus, if the water depth is less than the boulder height (i.e., the boulder is in the partially submerged condition), the lift force can be assumed to be zero.

Friction force,

$$F_f = -C_f\{vol_b(\rho_b - \rho)g\cos\alpha - F_l\}(U/U), \tag{5}$$

where C_f is the coefficient of friction between the bed and the contact surface of the boulder, g the gravitational acceleration (9.81 m/s^2), and ρ_b the density of the boulder. If $U \neq 0$, then $C_f = C_{df}$; otherwise, $C_f = C_{sf}$, where C_{df} is the coefficient of dynamic friction and C_{sf} the coefficient of static friction. If $vol_b(\rho_b - \rho)g\cos\alpha < F_l$, contact between the boulder and the bed is lost; this leads to $F_f = 0$ and therefore the boulder is transported due to saltation.

If the bed slope is gentle, $\cos\alpha$ can be approximated as

$$\cos\alpha \approx \sqrt{1-(\partial z/\partial x)^2} \tag{6}$$

Reduced gravity force,

$$F_g = vol_b(\rho_b - \rho)g \tag{7}$$

2.1.1. Boulder in submerged condition ($h > h_b$)

The momentum equation can be derived in such a way that the net force acting on the boulder is equal to the momentum changes of the boulder per unit of time as follows:

$$\begin{aligned}&(\rho_b^* + C_a)vol_b(dU/dt) - (1+C_a)vol_b(Du/Dt) - (C_d A_D/2)|u-U|(u-U)\\ &+ vol_b(\rho_b^* - 1)g(\partial z/\partial x) + C_f\left\{vol_b(\rho_b^* - 1)g\sqrt{1-(\partial z/\partial x)^2}\right.\\ &\left.-(C_l A_l/2)(u-U)^2\right\}(U/|U|) = 0,\end{aligned} \tag{8}$$

where $\rho_b^* = \rho_b/\rho$.

2.1.2. Boulder in partially submerged condition ($h_b > h > 0$)

When a boulder is transported in a partially submerged condition, the flow pattern around the boulder is rather chaotic compared to that in a submerged condition. The impact of the boulder on water is also significant; thus, the water depth

around the boulder varies significantly and the flow exhibits characteristics of turbulence. However, simplifying the complexity associated with turbulence, Eq. (8) can be revised for the partially submerged condition by imposing the ratio of water depth to boulder height as follows. The lift force is omitted

$$\{\rho_b^*+C_a(h/h_b)\}vol_b(dU/dt)-(1+C_m)(h/h_b)vol_b(Du/Dt) -(C_dA_dh/2h_b)|u-U|(u-U)-vol_b(\rho_b^*-h/h_b)g(\partial z/\partial x) +C_fvol_b(\rho_b^*-h/h_b)g\sqrt{1-(\partial z/\partial x)^2}(U/|U|)=0. \quad (9)$$

2.1.3. Subaerial boulder (not in contact with fluid)

The boulder is subjected to friction force and self-weight. The momentum equation can be derived as

$$dU/dt+g(\partial z/\partial x)+C_fg\sqrt{1-(\partial z/\partial x)^2}(U/|U|)=0. \quad (10)$$

2.1.4. Tsunami-induced flow

Depth-integrated shallow water equations are used to simulate tsunami propagation in the ocean and run up on the ground. The equations are written as follows.

Continuity equation for water

$$\partial\varsigma/\partial t+\partial Q/\partial x=0. \quad (11)$$

Momentum equation for water

$$\partial Q/\partial t+\frac{\partial(Q^2/h)}{\partial x}+gh(\partial\varsigma/\partial x)+\tau/\rho=0, \quad (12)$$

where Q is the discharge per unit width ($=uh$), and τ the bed roughness on water, $\tau=\rho gn_m^2Q^2/h^{7/3}$,where n_m is Manning's roughness coefficient.

Therefore, Eqs. (8)–(12) govern the transport of a boulder by a tsunami-induced force (long period wave).

2.2. Numerical discretization of governing equations

An explicit finite difference numerical scheme is proposed to solve the system of governing equations. The staggered method for variables in space and the leapfrog method for variables in time are adopted.

Governing equations are discretized as follows.

Continuity equation for water

$$\left(\varsigma_{i+1/2}^n-\varsigma_{i+1/2}^{n-1}\right)/\Delta t+\left(Q_{i+1}^{n-1/2}-Q_i^{n-1/2}\right)/\Delta x=0. \quad (13)$$

Momentum equation for water

$$\left(Q_i^{n+1/2}-Q_i^{n-1/2}\right)/\Delta t +\left(\alpha_1(Q_{i-1}^{n-1/2^2}/h_{i-1}^n)+\alpha_2(Q_i^{n-1/2^2}/h_i^n)+\alpha_3(Q_{i+1}^{n-1/2^2}/h_{i+1}^n)\right)/\Delta x +gh_i^n\left(\varsigma_{i+1/2}^n-\varsigma_{i-1/2}^n\right)/\Delta x+\left(gn_m^2/h_i^{n7/3}\right)\left|Q_i^{n-1/2}\right|\left(Q_i^{n+1/2}+Q_i^{n-1/2}\right)/2=0. \quad (14)$$

If $Q_i^{n-1/2}\geq 0$, then $\alpha_1=-1,\ \alpha_2=1,\ \alpha_3=0$ or else $\alpha_1=0$, $\alpha_2=-1,\alpha_3=1$.

Momentum equation for the boulder:

Submerged condition ($h>h_b$)

$$(\rho_b^*+C_a)vol_b((U^{n+1/2}-U^{n-1/2})/\Delta t) -(1+C_a)vol_b\left[\left(u_{cb}^{n+1/2}-u_{cb}^{n-1/2}\right)/\Delta t+u_{cb}^n(\alpha_1u_{cb-dx}^n+\alpha_2u_{cb}^n+\alpha_3u_{cb+dx}^n)/\Delta x\right] -(C_dA_D/2)|u_{cb}^n-U^{n-1/2}|\left\{u_{cb}^n-(U^{n+1/2}+U^{n-1/2})/2\right\} +vol_b(\rho_b^*-1)g\left(z_{j+1}^n-z_j^n\right)/\Delta x +C_f\left[vol_b(\rho_b^*-1)g\sqrt{1-\left\{\left(z_{j+1}^n-z_j^n\right)/\Delta x\right\}^2}\right. -(C_lA_l/2)\left(u_{cb}^n-U^{n-1/2}\right)\left\{u_{cb}^n-(U^{n+1/2}+U^{n-1/2})/2\right\}\Big] \times(U^{n-1/2}/|U^{n-1/2}|)=0 \quad (15)$$

Partially submerged condition ($h_b>h>0$)

$$\{\rho_b^*+C_a(h_{cb}^n/h_b)\}vol_b(U^{n+1/2}-U^{n-1/2})/\Delta t -(1+C_m)(h_{cb}^n/h_b)vol_b\left[\left(u_{cb}^{n+1/2}-u_{cb}^{n-1/2}\right)/\Delta t +u_{cb}^n(\alpha_1u_{cb-dx}^n+\alpha_2u_{cb}^n+\alpha_3u_{cb+dx}^n)/\Delta x\right] -(C_dA_dh_{cb}^n/2h_b)|u_{cb}^n-U^{n-1/2}|\left\{u_{cb}^n-(U^{n+1/2}+U^{n-1/2})/2\right\} +vol_b(\rho_b^*-h_{cb}^n/h_b)g\left(z_{j+1}^n-z_j^n\right)/\Delta x +C_fvol_b(\rho_b^*-h_{cb}^n/h_b)g\sqrt{1-\left\{\left(z_{j+1}^n-z_j^n\right)/\Delta x\right\}^2} \times(U^{n-1/2}/|U^{n-1/2}|)=0. \quad (16)$$

Body on a dry bed without fluid interaction ($h=0$)

$$(U^{n+1/2}-U^{n-1/2})/\Delta t+g\left(z_{j+1}^n-z_j^n\right)/\Delta x +C_fg\sqrt{1-\left\{\left(z_{j+1}^n-z_j^n\right)/\Delta x\right\}^2}(U^{n-1/2}/|U^{n-1/2}|)=0 \quad (17)$$

where $j=trunc(X/\Delta x)$, and X is the distance to the center point of the boulder from a datum (wave generation boundary; $x=0$).

In order to maintain the accuracy and stability of the results of the proposed scheme, the following conditions are applied. If $u_{cb}^n\geq 0$, then $\alpha_1=-1,\ \alpha_2=1,\ \alpha_3=0$, and otherwise, $\alpha_1=0,\ \alpha_2=-1,\ \alpha_3=1$. If $U^{n-1/2}=0$, then $C_f=C_{sf}$; otherwise, $C_f=C_{df}$, where i,j are the positions in space, n the position in time, h_{cb} the water depth near the boulder, and u_{cb} the current velocity near the boulder.

The numerical simulation is started by solving the continuity equation, followed by computing the momentum equation for water. Then, the current velocity and water depth near the boulder are used to solve the momentum equation for the boulder. Linear interpolation (Eq. (18)) is used to find the water depth and current velocity near the boulder (Fig. 2)

$$f_{cb}^n=f_i^n+\frac{f_{i+1}^n-f_i^n}{\Delta x}(X-i\Delta x). \quad (18)$$

To start the motion of the boulder, either the net driving force (in this study, vector summation of drag, inertia, and if the boulder is on a slope, the reduced gravity component) on the boulder must exceed the static friction between the contact surface of the boulder and the bed (i.e., motion in sliding) or the lift force must exceed the reduced gravity force on the boulder (i.e., motion in saltation). If each condition above is satisfied, the momentum equation for the boulder is used to calculate the velocity of the boulder, and consequently the new position is calculated.

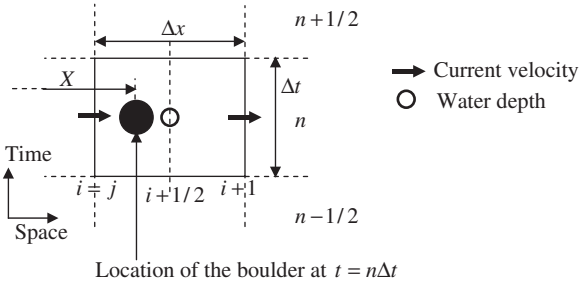

Fig. 2. Detailed sketch of a computation cell at $(i+1/2, n)$. The current velocity is calculated at the edge of the cell while the water depth is computed at the middle of the cell.

3. Calcareous boulders detached from a seawall by the 2004 Indian Ocean tsunami

The 2004 Indian Ocean tsunami unleashed its gigantic power on the coastal area of Lhok Nga (west of Banda Aceh city), turning the coastal environment upside down within a short time. It consisted of successive waves (eyewitnesses reported 3–10 waves; Lavigne et al., 2009): the first wave was less than 5 m, and the second and highest wave was 15–30 m at the coast, while very few observations were available for the following waves. The tsunami was also able to detach and transport three types of megaclasts: (1) hundreds of calcareous boulders up to 7.7 tons were lifted from a seawall and deposited up to 200 m inland, (2) mega-slabs of conglomerate weight up to 85 tons were dislodged from the tidal flat and deposited close to the shoreline in an overturned position, and (3) coral boulders (up to 11 tons) from the fringing reef were deposited as far as 900 m inland (smaller coral boulders (<1 m) were found up to 1460 m inland). The boulders were assumed to be deposited by the second and highest wave, even if the backwash removed some boulders (Paris et al., 2010). We used our numerical model to simulate the transport of 12 calcareous boulders detached from a seawall by the tsunami and then discuss the simulated results in comparison with the field observations.

3.1. Could the first tsunami wave transport calcareous boulders from the seawall?

The seawall was constructed along the coast, and the tsunami bore was preceded by water withdrawal (Lavigne et al., 2009). Therefore, boulders of the seawall were in a subaerial condition before the first tsunami wave hit the seawall. Theoretically, the initial mode of transport of a boulder by tsunami flow could be sliding, rolling, or saltation (Nandasena et al., in press). Initial transport modes of sliding and saltation are neglected: boulder-to-boulder interlocking in the seawall could prevent sliding and the higher current velocity required for saltation. Thus, the threshold current velocity necessary to initiate transport of a subaerial boulder by overturning is considered.

The initial transport of a boulder will be rolling/overturning when

$$M_d + M_l + M_m \geq M_r \tag{19}$$

$$M_d = 0.5\rho_w C_d(ah_b)u^2(h_b/2) \tag{20}$$

$$M_l = 0.5\rho_w C_l(ab)u^2(b/2) \tag{21}$$

$$M_m = \rho_w C_m(abh_b)du/dt(h_b/2) \tag{22}$$

$$M_r = (\rho_s - \rho_w)(abh_b)g(b/2) \tag{23}$$

$$u^2 \geq \left\{\frac{(\rho_s/\rho_w - 1)g}{C_m(h_b/b)} - \frac{du}{dt}\right\} \Big/ \left\{\frac{C_d(h_b^2/b^2)+C_l}{2C_m(h_b^2/b^2)}\right\} \tag{24}$$

where M_d, M_l, M_m, and M_r are moments of drag, lift, inertia, and restraint (reduced gravity), respectively, applied to the boulder, u is the current velocity, ρ_s the boulder density (2400 kg/m^3), ρ_w the density of seawater (1020 kg/m^3), b and h_b the boulder length (intermediate, and short), and g the gravitational acceleration (9.81 m/s^2). We do not have in situ force coefficients for the boulders and field concerned; therefore, the coefficients used in past studies were adopted: C_d is the coefficient of drag (1.95; Noormets et al., 2004; Paris et al., 2010), C_l the coefficient of lift (0.178; Nott, 1997, 2003; Noormets et al., 2004; Paris et al., 2010), and C_m=coefficient of inertia (2.0; Nott, 2003). Nott (2003) introduced a method to solve Eq. (24) for minimum current velocity (u) by assuming a conservative value for flow acceleration (du/dt). This method is not practical because we do not know the exact flow acceleration, and it could produce unrealistic results (Nandasena et al., in press). Goto et al. (2010) and Tanaka et al. (2009) noted that the drag force would be significant compared to the inertia force (see Fig. 10 for our results). The first tsunami wave was significantly smaller than the second tsunami wave (highest). Therefore, we omitted the inertia force when analyzing the first tsunami wave but considered it for the second wave. Eq. (24) can be rearranged without inertia force

$$u^2 \geq \frac{2(\rho_s/\rho_w - 1)h_b g}{C_d(h_b^2/b^2)+C_l}. \tag{25}$$

The possibility of initial transport of calcareous boulders by the first tsunami wave was tested by Eq. (25). The minimum current velocity to initiate boulder transport ranges from 3.3 to 5.4 m/s (Table 1), but, in reality, the current velocity range would be higher than the calculated range as boulder-to-boulder interlocking in the seawall could provide additional resistance to the motion. The first tsunami wave at the shoreline was less than 5 m (Paris et al., 2009). Eyewitness accounts collected by Lavigne et al. (2009) confirmed that the boulders were moved by the second and highest wave, even if the first wave could have destabilized the seawall, thus preparing the boulders for transport by the following waves.

3.2. Numerical simulation (the second and highest tsunami wave)

The direction of current velocity was almost perpendicular to the shore when the tsunami hit the seawall (Paris et al., 2009). Therefore, the numerical model introduced here can be used to simulate the boulder transport assuming two-dimensional effects are minimal. Tides are very low in Lhok Nga (see Lavigne et al. (2009) for more details), and this is a trivial parameter in comparison to tsunami wave heights. Therefore, bed elevations were measured perpendicular to the shore (Fig. 3) with respect to the mean sea level (Fig. 4). The wave generation boundary at water depth of 200 m was rather arbitrarily selected and one sinusoidal wave with a 20-min period was considered. Discretization sizes of distance and time for numerical simulation dx=5 m and dt=0.056 s were selected, while friction coefficients C_{sf}=0.8 and C_{df}=0.7 (Imamura et al., 2008), the added mass coefficient, C_a=1.0 (Nott, 2003), and Manning's roughness, n_m=0.025 (Harada and Imamura, 2006) were used. The amplitude of the wave at the wave generation boundary was determined by an iterative process such that the tsunami wave conditions (water

Table 1
Simulated minimum current velocity to initiate the boulder transport.

Boulder ID	Axis length (m)			Density kg/m^3	u_{min} (m/s) from Eq. (25)
	a	b	h_b		
B1	2.35	1.75	1.50	2400	5.0
B2	3.30	1.70	1.10	2400	5.4
B3	2.10	1.35	1.30	2400	4.2
B4	1.85	1.35	1.10	2400	4.5
B5	1.60	1.25	1.20	2400	4.0
B6	1.40	1.40	1.30	2400	4.3
B7	1.70	1.40	1.00	2400	4.8
B8	1.80	1.10	1.00	2400	3.9
B9	1.00	0.95	0.95	2400	3.4
B10	1.30	1.10	0.85	2400	4.1
B11	1.70	1.10	0.55	2400	4.7
B12	0.82	0.80	0.70	2400	3.3

Values are in agreement with velocities proposed in the literature for the same study area (3–8 m/s) (Lavigne et al., 2009; Paris et al., 2010).

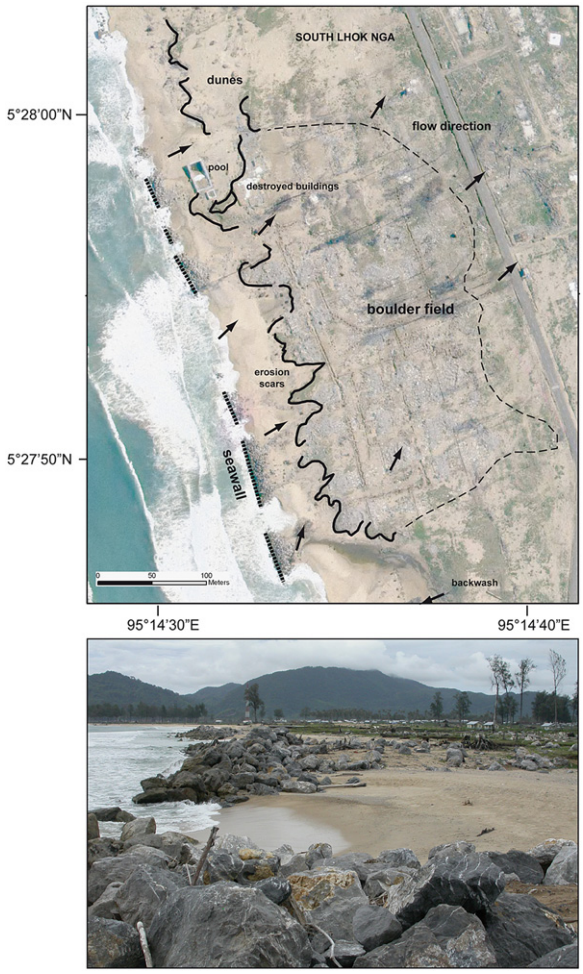

Fig. 3. Aerial orthorectified photo (June 2005) of south Lhok Nga, showing the calcareous boulder field ($N=1000$ boulders) and erosion escarpments behind the seawall (modified after Paris et al. (2009)). Note that the erosional insets and boulder concentrations are in the axes of the trenches cut by the tsunami in the seawall.

depth and current velocity) at the shore were similar to field observations and previous numerical studies (Paris et al., 2009): the second and largest wave with a turbulent bore came from the west–southwest direction and was 15–30 m at the coast. Numerical modeling and analysis of videos gave tsunami flow velocities increasing from 3 to 12 m/s from the coral boulder fields offshore to the coast (Fritz et al., 2006; Paris et al., 2010). These data could have errors because they are not direct measurements. However, our numerical results agree fairly well with these observations (Fig. 5). The numerical results also show the so-called tsunami bore front at the shoreline.

3.3. Results and discussion

Fig. 6 displays simulated transport distance compared to observed distance due to the second and highest tsunami wave. A few field observations match the simulated results. Most of the observed distances are less than the simulated values. This infers that the energy boulders received from the tsunami were dissipated by means other than transport. Most likely, boulder-to-boulder interaction at the beginning of the transport would have a major impact on reduction in transport distance, dissipating its energy in impulses as the destruction of the seawall set free different-sized boulders whose velocities also differed from

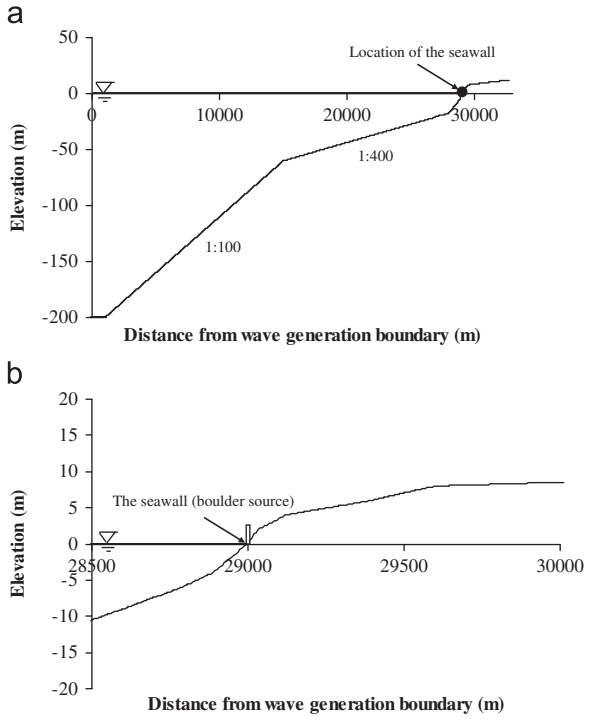

Fig. 4. (a) Bed elevations measured from mean sea level along a line perpendicular to the shore. Wave generation boundary is assumed at the water depth of 200 m and (b) close-up view: bed elevations near the shoreline. The seawall is the boulder source.

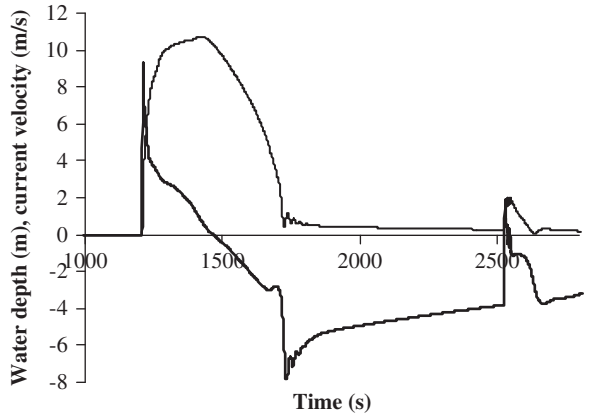

Fig. 5. Temporal variations of hydraulic properties of the tsunami at the shoreline: thick line for current velocity and thin line for water depth.

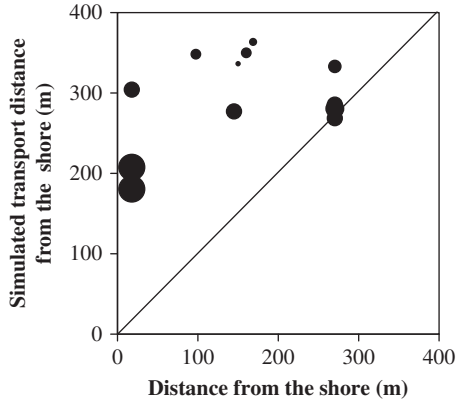

Fig. 6. Transport distance measured from the shore; the size of a dot is proportional to its weight. Numerical results indicate the net transport distance because some boulders showed backward motion (Fig. 7).

one another (Fig. 3, lower photograph). Boulder-to-boulder interactions were evidenced by striae, percussive marks, or crushing on the surface of the boulders (see Paris et al., 2009).

B5 and B6 have roughly the same weight, but their transport distances measured in the field are rather different. Perhaps these differences are due to either the effect of collision or surface microtopographical effects, which can completely stop the transport prematurely (e.g., some boulders were trapped in a swimming pool near the seawall; Paris et al. (2009). Goto et al. (2010) also revealed that spatial and grain size distributions are strongly controlled by the initial distribution of boulders at the source as well as the hydrodynamic features of the tsunami and local topography.

The transport distance and direction (landward/shoreward) were greatly influenced by the subjecting flow field (current velocity/water depth). In simulated results (Figs. 7 and 8) boulders B1 and B8–12 show both landward and shoreward motions that would imply two stops during their transport: the first stop occurred during the inflow–outflow transition, and the second one at the final stage of the backwash. The landward transport distance is large compared to the shoreward movement, exemplifying the strong overland flow velocities that are a function of the tsunami period and amplified tsunami height due to shoaling. Boulders B2–7 show only landward motion as the backwash was not strong enough to cause the secondary motion. Tsunami run-up and boulder transport distance can show a large

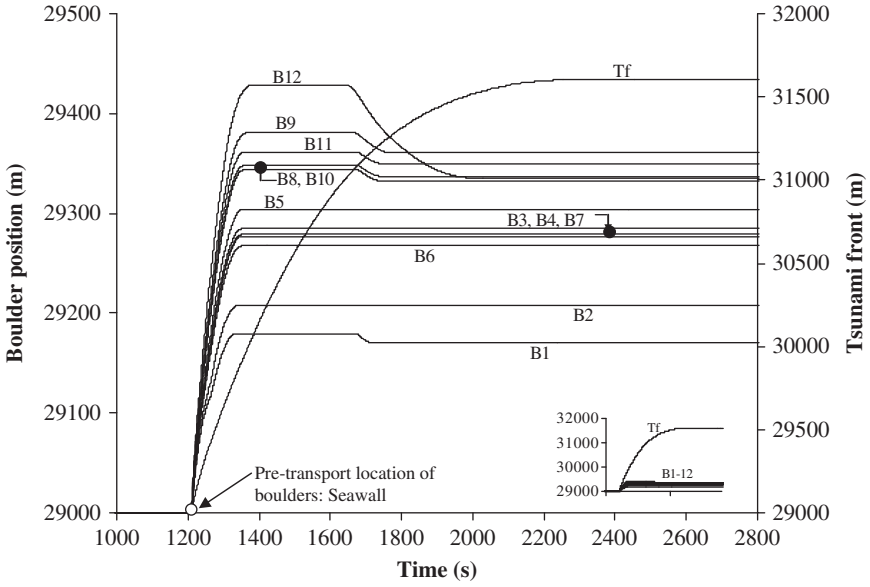

Fig. 7. Boulder trajectory in comparison with moving tsunami front. Inset: plot on same scale. At $t=1208$ s, the tsunami front hit the seawall. Tf, tsunami front.

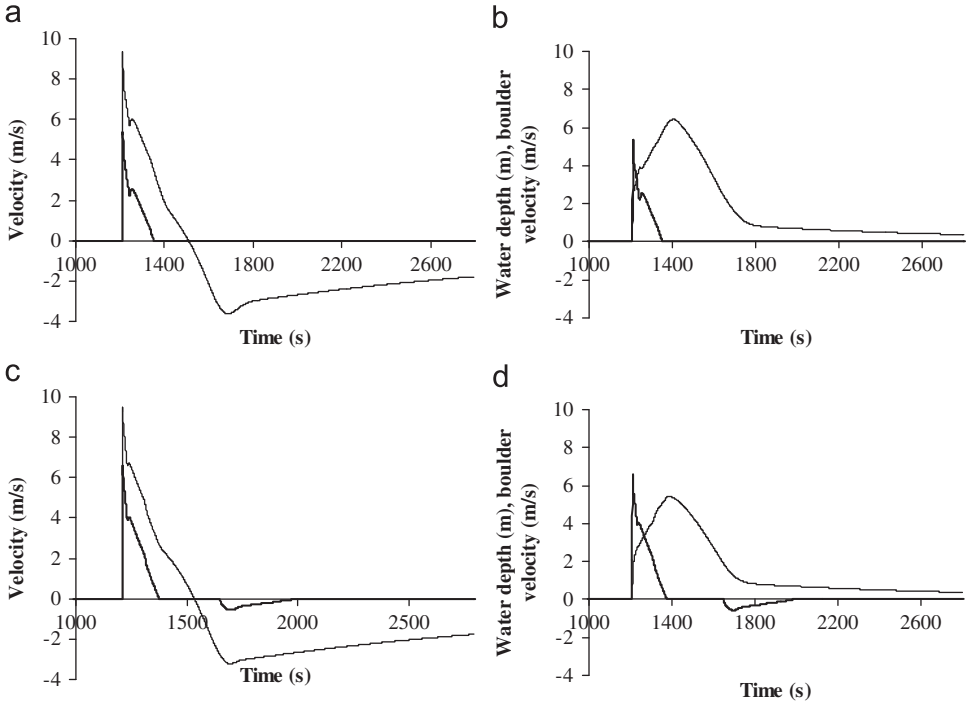

Fig. 8. Temporal variations of boulder velocity, current velocity, and water depth near the boulder (a and b) for B3, (c and d) for B12. Note thick line for boulder and thin line for tsunami.

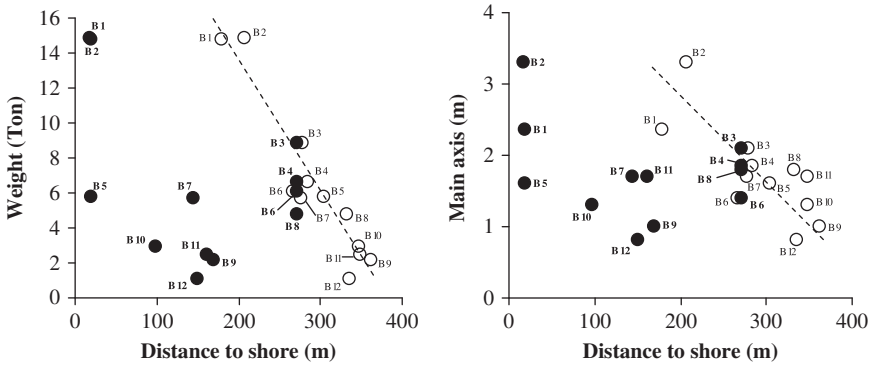

Fig. 9. Landward fining: field investigation (black circle) and numerical simulation (white circle).

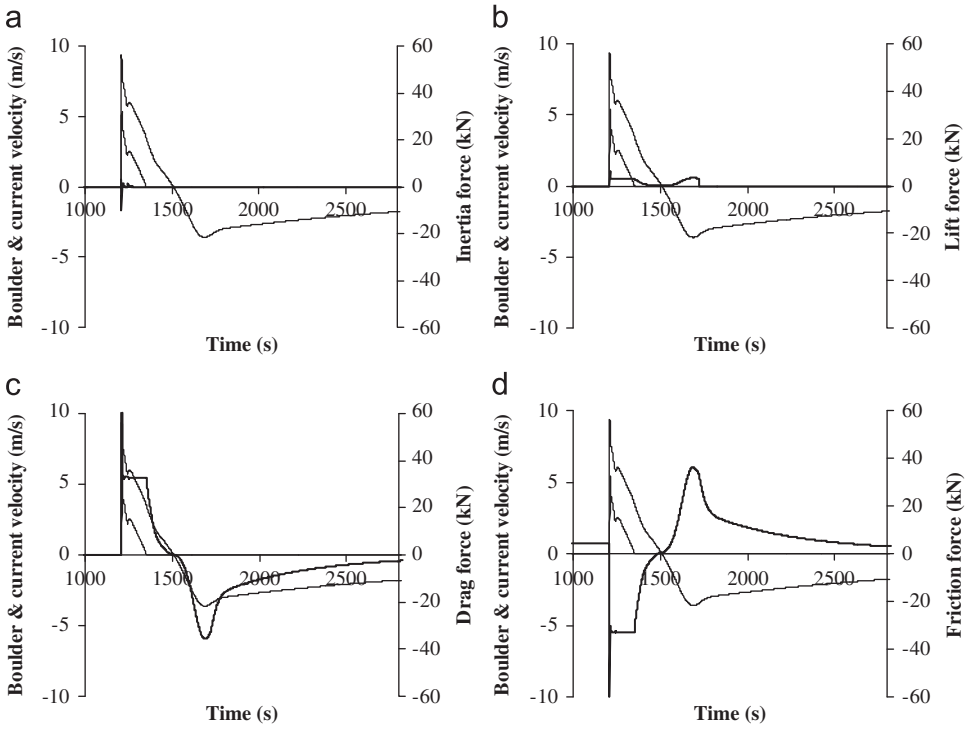

Fig. 10. Force history applied to B3: (a) inertia force, (b) lift force, (c) drag force, and (d) friction force; thick line indicates force.

difference; thus, it is not reliable to use the location of historic boulder deposits to directly infer tsunami run-ups (Fig. 7, inset).

No landward fining was found for the observed field boulder transport distances, whereas the simulated distances show a reasonable relationship for weight and main axis against the distance measured from the shoreline (Fig. 9). We suggest that the main reasons for the lack of landward fining are boulder-to-boulder impact, the influence of surface microtopographical effects, and the effect of backwash.

Numerical results reveal that drag and friction are the dominant forces compared to lift and inertia forces during boulder transport (Fig. 10). A uniform drag force is observed during boulder transport. The inertia force is dependent on the magnitude of acceleration of tsunami currents. Even though the contribution from lift force is small, it would make the transport easier by reducing the friction force. When a boulder is not transported by the current force the total driving force is resisted by the static friction force. It highlights the need for drag and friction coefficients to be determined more precisely than the others when using the numerical model to determine the boulder transport as the effect of these forces are dominant.

4. Conclusions

Governing equations for boulder transport by tsunamis in submerged, partially submerged, and subaerial conditions were derived from Nott's original equations (1997, 2003). A new numerical solution to the governing equations was proposed. Then the numerical model was used to simulate the transport of calcareous boulders detached from a seawall by the 2004 Indian Ocean tsunami in Lhok Nga, Sumatra, Indonesia. A few simulated transport distances matched the field observations, but other simulated distances are larger than the field measurements. Clast-to-clast interaction would have a major impact on the reduction of transport distance by dissipating the energy in impulses because destruction of the seawall set free different-sized boulders with different velocity to weight ratios. However, this is marginal. In addition, surface

microtopographical effects could have stopped transport prematurely. Addressing these types of complex local factors in numerical modeling is far beyond the scope of this study. Bridging the gap between predictions by theory-based numerical simulations and real observations could be viable through empirical relations. No landward fining was observed in the field measurements, but the numerically predicted results showed a reasonable trend toward landward fining. Numerical results reveal that drag and friction are the dominant forces applied to boulders during transport, and therefore, accurate estimation of drag and friction coefficients is also important for validation of the model. The difference between the simulated results and field observations is partly attributable to limitations of the numerical model, which are listed below:

1. A boulder is considered to be a homogeneous cubic/or rectangular prism. The initial orientation of a boulder considers that the long axis of the boulder is perpendicular to the tsunami direction; thus, the model assumes constant drag and lift areas during the transport.
   A boulder in the field is neither cubic nor rectangular and heterogeneous; thus the numerical model usually underestimates or overestimates its weight. As the boulder is subjected to complex motion, fixed projected areas for force calculation are not always conservative. Lorang (2000) simulated different boulder movements and found that transportability was strongly influenced by the boulder shape.
2. The pretransport environment of a boulder is important (Pignatelli et al., 2009; Goto et al., 2010), but the model simplifies the boulder to be isolated (single), detached, and not buttressed.
3. Previous models of boulder transport assumed sliding as a mode of transport for a boulder (Noji et al., 1993; Imamura et al., 2001), but boulders in the experiments of Imamura et al. (2008) are mainly seen to be transported by a bore due to rolling or saltation rather than by sliding. Experimental studies showed that the transport mode can vary depending on the current velocity, bottom friction, and shape and weight of the boulder (Goto and Imamura, 2007). Our new model takes sliding and saltation into account. Rolling is a very complex phenomenon. One approach is to consider rolling in the model by reducing dynamic friction. This is not theoretical, but uses extensive experimental studies to develop an empirical relationship (e.g., Imamura et al. (2008) found such a relationship by doing limited experimental studies). The other approach is to consider the concept of angular momentum. This is theoretical. In this case, the hydraulic moment is more appropriate than hydraulic force applied to a boulder to calculate the boulder velocity and transport distance.
4. Constant force coefficients are used in the numerical simulation, and they are obtained from past studies. As in Noji et al. (1993), these coefficients are time dependent and functions of the Froude number and relative water depth. Therefore, a precise estimation of these coefficients at the site concerned should be attempted.
5. Boulder-to-boulder interactions (collisions and shielding effects) are disregarded. These interactions during boulder transport, as evidenced by striae, percussive marks, or crushing on the surface of the boulders, were observed by Paris et al. (2009) during a field survey in January 2005.
6. The depth-averaged flow structure around the boulder is considered and the model disregards the microtopographical changes, but these parameters could be important in boulder transport.

These limitations remain to be overcome in future studies, and the model will be enhanced to two or three dimensions for an advanced discussion of the subject matter.

Acknowledgments

We thank an anonymous reviewer, Brian G. Jones, and Eric C. Grunsky for providing very useful comments and suggestions to improve the original manuscript. R. Paris is funded by ANR project Risknat-Maremoti.

References

Barbano, M.S., Pirrotta, C., Gerardi, F., 2010. Large boulders along the south-eastern Ionian coast of Sicily: storm or tsunami deposits? Marine Geology 275, 140–154.
Benner, R., Browne, T., Brückner, H., Kelletat, D., Scheffers, A., 2010. Boulder transport by waves: progress in physical modelling. Zeitschrift für Geomorphologie 54, 127–146.
Bourgeois, J., Mac Innes, B., 2010. Tsunami boulder transport and other dramatic effects of the 15 November 2006 central Kuril Islands tsunami on the island of Matua. Zeitschrift für Geomorphologie 54, 175–195.
Etienne, S., Paris, R., 2010. Boulder accumulations related to storms on the south coast of the Reykjanes Peninsula (Iceland). Geomorphology 114, 55–70.
Fritz, H.M., Borrero, J.C., Synolakis, C.E., Yoo, J., 2006. 2004 Indian Ocean tsunami flow velocity measurements from survivor videos. Geophysical Research Letters 33, L24605.
Goff, J., Weiss, R., Courtney, C., Dominey-Howes, D., 2010. Testing the hypothesis for tsunami boulder deposition from suspension. Marine Geology 277, 73–77.
Goto, K., Imamura, F., 2007. Numerical models for sediment transport by tsunamis. The Quaternary Research (Daiyonki-Kenkyo) 46, 463–475.
Goto, K., Okada, K., Imamura, F., 2009a. Characteristics and hydrodynamics of boulders transported by storm waves at Kudaka Island, Japan. Marine Geology 262, 14–24.
Goto, K., Okada, K., Imamura, F., 2009b. Importance of the initial waveform and coastal profile for tsunami transport of boulders. Polish Journal of Environmental Studies 18, 53–61.
Goto, K., Okada, K., Imamura, F., 2010. Numerical analysis of boulder transport by the 2004 Indian Ocean tsunami at Pakarang Cape, Thailand. Marine Geology 268, 97–105.
Hall, A.M., Hansom, J.D., Williams, D.M., 2010. Wave-emplaced coarse debris and megaclasts in Ireland and Scotland: boulder transport in a high-energy littoral environment: a discussion. Journal of Geology 118, 699–704.
Hansom, J.D., Barltrop, N.D.P., Hall, A.M., 2008. Modelling the processes of cliff-top erosion and deposition under extreme storm waves. Marine Geology 253, 36–50.
Harada, K., Imamura, F., 2006. Effects of coastal forest on tsunami hazard mitigation—A preliminary investigation. In: Satake, K. (Ed.), Tsunamis: Case Studies and Recent Development, Advances in Natural and Technological Hazards Research. Springer, Dordrecht, The Netherlands, pp. 279–292.
Imamura, F., Goto, K., Ohkubo, S., 2008. A numerical model of the transport of a boulder by tsunami. Journal of Geophysical Research 113, C01008.
Imamura, F., Yoshida, I., Moore, A., 2001. Numerical study of the 1771 Meiwa tsunami at Ishigaki Island, Okinawa, and the movement of the tsunami stones. Japan Coastal Engineering Journal JSCE 48, 346–350.
Kennedy, D.M., Tannock, K.L., Crozier, M.J., Rieser, U., 2007. Bolder of MIS 5 age deposited by a tsunami on the coast of Otago, New Zealand. Sedimentary Geology 200, 222–231.
Kogure, T., Matsukura, Y., 2010. Instability of coral limestone cliffs due to extreme waves. Earth Surface Processes and Landforms 35, 1357–1367.
Lange, W.P., de Lange, P.J., de Moon, V.G., 2006. Boulder transport by waterspouts: an example from Aorangi Island, New Zealand. Marine Geology 230, 115–125.
Lavigne, F., Paris, R., Grancher, D., Wassmer, P., Brunstein, D., Vautier, F., Leone, F., Flohic, F., De Coster, B., Gunawan, T., Gomez, Ch., Setiawan, A., Cahyadi, R., Fachrizal, 2009. Reconstruction of tsunami inland propagation on December 26, 2004 in Banda Aceh, Indonesia, through field investigations. Pure and Applied Geophysics 166, 259–281.
Lorang, M., 2000. Predicting the threshold entrainment mass for a boulder. Journal of Coastal Research 16 (2), 432–445.
Lorang, M., in press. A wave-competence approach to distinguish between boulder and megaclast deposits due to storm waves versus tsunamis. Marine Geology, doi:10.1016/j.margeo.2010.10.005.
Luccio, P.A., Voropayev, S.I., Fernando, H.S.J., Boyer, D.L., Houston, W.N., 1998. The motion of cobbles in the swash zone on an impermeable slope. Coastal Engineering 33, 41–60.
Maouche, S., Morhange, C., Meghraoui, M., 2009. Large boulder accumulation on the Algerian coast evidence tsunami events in the western Mediterranean. Marine Geology 262, 96–104.
Mastronuzzi, G., Sanso, P., 2004. Large boulder accumulations by extreme waves along the Adriatic coast of southern Apulia (Italy). Quaternary International 120, 173–184.
Mhammdi, N., Medina, F., 2008. Large boulders along the Rabat Coast (Morocco); possible emplacement by the November, 1st, 1775 A.D. Tsunami. Science of Tsunami Hazards 27 (1), 17–30.
Morton, R.A., Richmond, B.M., Jaffe, B.E., Gelfenbaum, G., 2006. Reconnaissance investigation of Caribbean extreme wave deposits—preliminary observations, interpretations, and research directions. U.S. Geological Survey Open-File Report 2006-1293, 46 pp (PDF). URL: 〈http://pubs.usgs.gov/of/2006/1293/〉.

Nandasena, N.A.K., Paris, R., Tanaka, N., in press. Reassessment of hydrodynamic equations: minimum flow velocity to initiate boulder transport by high energy events (storms, tsunamis). Marine Geology, doi:10.1016/j.margeo.2011.02.005.

Noji, M., Imamura, F., Shuto, N., 1993. Numerical simulation of movement of large rocks transported by tsunamis. In: Proceedings of IUGG/IOC International Symposium. Wakayama, Japan, pp. 189–197.

Noormets, R., Crook, K.A.W., Felton, E.A., 2004. Sedimentology of rocky shorelines: 3. hydrodynamics of megaclast emplacement and transport on a shore platform, Oahu, Hawaii. Sedimentary Geology 172, 41–65.

Nott, J., 1997. Extremely high wave deposits inside the Great Barrier Reef, Australia: determining the cause-tsunami or tropical cyclone. Marine Geology 141, 193–207.

Nott, J., 2003. Waves, coastal boulders and the importance of the pre-transport setting. Earth and Planetary Science Letters 210, 269–276.

Nott, J., 2004. The tsunami hypothesis—comparison of the field evidence against the effects, on the Western Australian coast, of some of the most powerful storms on earth. Marine Geology 208, 1–12.

Paris, R., Fournier, J., Poizot, E., Etienne, S., Morin, J., Lavigne, F., Wassmer, P., 2010. Boulder and fine sediment transport and deposition by the 2004 tsunami in Lhok Nga (western Banda Aceh, Sumatra, Indonesia): a coupled offshore-onshore model. Marine Geology 268, 43–54.

Paris, R., Wassmer, P., Sartohadi, J., Lavigne, F., Barthomeuf, B., Desgages, É., Grancher, D., Baumert, Ph., Vautier, F., Brunstein, D., Gomez, Ch., 2009. Tsunamis as geomorphic crisis: lessons from the December 26, 2004 tsunami in Lhok Nga, west Banda Aceh (Sumatra, Indonesia). Geomorphology 104, 59–72.

Pignatelli, C., Sanso, P., Mastronuzzi, G., 2009. Evaluation of tsunami flooding using geomorphologic evidence. Marine Geology 260, 6–18.

Scheffers, A., Kelletat, D., Vött, A., May, S.M., Scheffers, S., 2008. Large Holocene tsunami traces on the western and southern coastlines of the Peloponnesus (Greece). Earth and Planetary Science Letters 269, 271–279.

Scicchitano, G., Monaco, C., Tortorici, L., 2007. Large boulder deposits by tsunami waves along the Ionian coast of south-eastern Sicily (Italy). Marine Geology 238, 75–91.

Spiske, M., Borocz, Z., Bahlburg, H., 2008. The role of porosity in discriminating between tsunami and hurricane emplacement of boulders—a case study from the Lesser Antilles, southern Caribbean. Earth and Planetary Science Letters 268, 384–396.

Switzer, A.D., Burston, J.M., 2010. Competing mechanisms for boulder deposition on the southeast Australian coast. Geomorphology 114, 42–54.

Tanaka, N., Nandasena, N.A.K., Jinadasa, K.S.B.N., Sasaki, Y., Tanimoto, K., Mowjood, M.I.M., 2009. Developing effective vegetation bioshields for tsunami protection. Journal of Civil and Environmental Engineering Systems 26, 163–180.

Williams, D.M., Hall, A.M., 2004. Cliff-top megaclast deposits of Ireland, a record of extreme waves in the North Atlantic-storms or tsunamis? Marine Geology 206, 101–117.